2 LITERATURE SURVEY

2.1 Properties and Uses of Titanium Metal and Its Oxides.

Titanium dioxide reflects and scatters light in the visible spectrum like thousands of tiny mirrors. This means that, when it is incorporated in paints, plastics or paper, it imparts brilliance and opacity to these products (Minkler and Baroch, 1981; Richards Bay Minerals). Unlike poisonous lead compounds, which may also be used to give the white and bright colour, TiO_2 is non-poisonous, non-toxic, and biologically inert. TiO_2 absorbs the dangerous ultraviolet (UV) rays from the sun, hence it is used in modern sunscreen to prevent skin cancer. Rutile is also used in welding rod fluxes. It stabilizes the arc and protects the molten metal from oxidation during welding, hence forming a superior welding joint (Richards Bay Minerals; Fisher, 1997). It is also used in certain metallurgical and electronic applications and extensively in surface coatings (Fisher, 1997). Finally, it is used in the manufacture of titanium metal. Due to the excellent properties of the metal (lightness, strength, corrosion resistance and heat resistance) it is used extensively in the aerospace industries. The lightness, strength and inert properties make it ideal for use in artificial hip joints, heart pace makers and spectacle frames (Minkler and Baroch, 1981; Richards Bay Minerals).

2.2. Titaniferous Feedstocks.

2.2.1. Feedstocks for the production of titanium tetrachloride.

The decision on which route to follow in transforming titanium ore (or upgraded ilmenite) to the pigment will depend on the purity level of the feedstock. The sulphate route has been used to process lower grade titanium feedstock. The chloride process requires significantly higher-grade titanium feedstock (van Dyk et al. 1999). This work will focus on titania slag produced from South Africa ilmenite with low impurity content. These impurities (such as MnO, MgO, CaO, Al_2O_3, and SiO_2) largely report to the slag, making up about 6% (by mass) of the total (Pistorius, 2002).

There are still large deposits of rutile in a limited number of places such as Australia, Sri Lanka, South Africa, India and Sierra Leone (Minkler and Baroch, 1981; van Dyk et. al. 1999). However, the price of rutile has quadrupled over the last twenty years. This resulted in a shift towards the use of substitute materials for natural rutile. Other abundant low-grade titanium minerals such as ilmenite ($FeTiO_3$), arizonite ($Fe_2O_3.nTiO_2.mH_2O$), leucoxene ($Fe_2O_3.nTiO_2$), perovskite ($CaTiO_3$) and titaniferous magnetite must be utilized as substitutes for rutiles. In South Africa, Richard Bay Minerals obtains its rutile and ilmenite from the coastal area of northern Kwazulu-Natal along the Zululand coast (Richards Bay Minerals). Namakwa Sands, which is an Anglo American company, uses a direct electric arc furnace in the smelting of ilmenite obtained from mineral sands on the western coast.

Due to the high level of impurities - especially iron - in these minerals, it is necessary to upgrade them to obtain synthetic rutile or other high-titanium feedstocks, which are acceptable for chlorination (Rhee and Sohn, 1990). High quality titania slag is also used in pigment production as a substitute for natural rutile. A number of processes have been proposed for the removal of iron from low-grade titanium ore (Minkler and Baroch, 1981). Typical compositions of rutile, ilmenite and high titania slag are given in table 2.2.

Table 2.2: Typical Composition Of Rutile, Ilmenite and High Titania Slag (Kahn, 1983; Minkler and Baroch, 1981)

Compounds	Rutile (USA) % by weight	Ilmenite (USA) % by weight	High titania slag (RBM) % by weight	Synthetic rutile (Western) % by weight
TiO_2	96.06[a]	64.6[a]	85.5[a]	92.8[a]
Ti_2O_3	-	-	25.0	10.0
Fe_2O_3	1.46	29.8	-	-
FeO	-	-	7.5	-
Fe (metallic)	-		0.2	
Fe (total)		20.8		2.1
MnO	-	-	1.4	1.0
Al_2O_3	0.33	0.62	2.0	1.1
SiO_2	-	0.26	1.5	1.2
ZrO_2	0.05	0.027	-	0.15
V_2O_5	-	0.22	0.40	0.02
Cr_2O_3	0.08	-	0.22	0.03
NbO_3	-	-	-	0.2
MgO	0.038	0.2	0.9	0.3
CaO	0.034	0.086	0.14	0.03
P_2O_5	0.09	0.16	-	0.02
C	-	-	0.07	0.3
S	-	-	0.06	0.3

a TiO_2 actually gives the total titanium content, expressed as TiO_2 (i.e. including both trivalent and tetravalent titanium).

2.2.2 Characterization Of Chlorinatable Titaniferous Feedstock

Environmental pressures on waste disposal are forcing pigment producers to use feedstocks with a higher content of TiO_2 and lower levels of trace elements. Manufacturers who use ilmenite directly once enjoyed a cost advantage. Nowadays this advantage is diminishing because of environmental concerns arising from the fact that a larger amount of iron waste product is generated from direct ilmenite use (Stanaway, 1994). Because the sulphate process produces

up to three times more waste than the chloride process, more effort now goes to supply the chloride producers where a volume growth of 40% is expected over the next 10 years (Stanaway, 1994). Recently, the demand for chlorinatable upgraded ilmenite (synthetic rutile), has began to rival that of natural rutile (van Dyk et. al. 1999). Pistorius and le Roux, (2002) reported that titania slag with 86.45-89.38mass% TiO_2 could also be chlorinated effectively.

2.2.3 Techniques for the Upgrading of Sub-Rutile feedstocks.

Due to ilmenite's wide geological distribution and price advantage over rutile, hundreds of techniques have been proposed for upgrading the TiO_2 content in ilmenite making it a more feasible feedstock for the generation of $TiCl_4$ (Minkler and Baroch, 1981; Kahn, 1983). Four main routes to the successful production of synthetic rutile from ilmenite are shown in figure 2.2.3 below (Kahn, 1983).

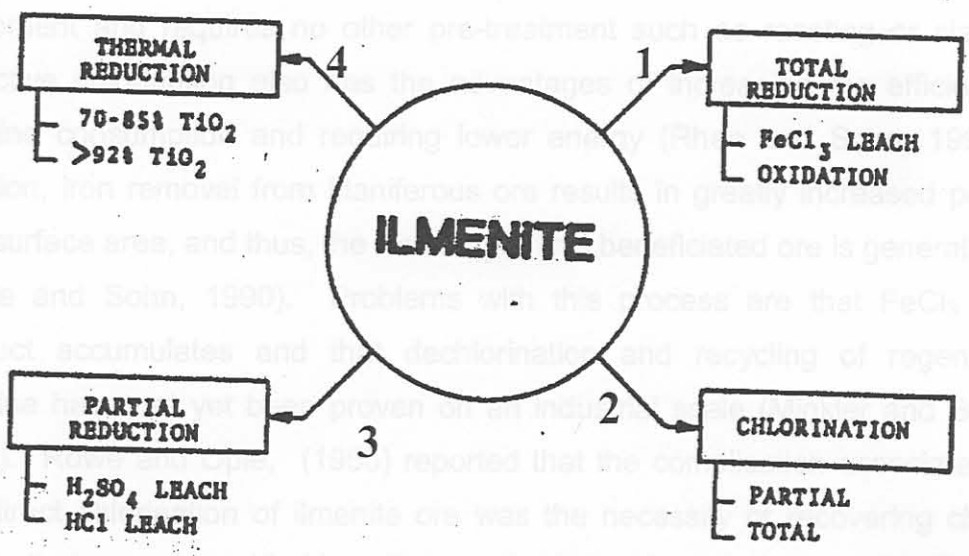

Figure 2.2.3: Possible Ilmenite to Rutile Routes (Kahn, 1983)

Route 1 is the Becher process, which involves a pre-oxidation step followed by total reduction of the ilmenite to metallic iron by coal in a rotary kiln (Minkler and Baroch, 1981; Kahn, 1983). The iron is then removed by agitating the metallized

ore in aerated water in the presence of a catalyst (NH_4Cl). The iron is oxidised and then separated from the leached ilmenite in a washing cyclone (Kahn, 1983). TiO_2 is acid leached to removed the ferrous oxide and dried to yield synthetic rutile (Minkler and Baroch, 1981). The leaching typically proceeds for 12-16 hours at 70-80^{o}C.

Route 2, known as the Dunn process, is based on the fact that iron in ilmenite chlorinates selectively and more readily than titanium. After pre-treatment, the ore is chlorinated in a fluidized-bed with an excess of ilmenite so that any titanium that chlorinates will react with the iron oxide and remain in the concentrate as TiO_2. The iron chloride gas leaving the bed is reacted with oxygen to form iron oxide and chlorine gas for recycling (Minkler and Baroch, 1981) and (Kahn, 1983). Under proper conditions, iron extraction is essentially complete before $TiCl_4$ production commences. Direct chlorination has a significant advantage in that it could be done in conventional chlorination equipment and requires no other pre-treatment such as roasting or slagging. Selective chlorination also has the advantages of increasing the efficiency of chlorine consumption and requiring lower energy (Rhee and Sohn, 1990). In addition, iron removal from titaniferous ore results in greatly increased porosity and surface area, and thus, the reactivity of this beneficiated ore is generally high (Rhee and Sohn, 1990). Problems with this process are that $FeCl_3$ waste product accumulates and that dechlorination and recycling of regenerated chlorine have not yet been proven on an industrial scale (Minkler and Baroch, 1981). Rowe and Opie, (1955) reported that the complication associated with the direct chlorination of ilmenite ore was the necessity of recovering chlorine values tied up as iron chlorides. Direct oxidation of $FeCl_3$ was not efficient, owing to its tendency to dissociate into the difficultly oxidisable $FeCl_2$. Other operational difficulties associated with the chlorination of titaniferous feedstocks are the defluidization and clogging caused by high-boiling point metal chlorides produced during chlorination (Rhee and Sohn, 1990). Nonetheless, these difficulties can be alleviated by the control of temperature, amount of reducing

agent and the partial pressure of chlorine. Another type of direct chlorination of the ore is the chlorination of both iron and titanium, forming volatile chlorides, which are subsequently separated (Rhee and Sohn, 1990).

Route 3, which is the Benelite process (Minkler and Baroch, 1981; Kahn, 1983), involves partial reduction of ilmenite with carbonaceous material in a rotary kiln, converting the ferric oxide (Fe_2O_3) to ferrous oxide (FeO). The reduced ilmenite is cooled and charged into a digester for leaching with 18-20% hydrochloric acid at 140^{O}C to give beneficiated ilmenite (synthetic rutile).

Route 4 is a viable approach and is usually performed by electric arc furnace smelting of ilmenite to produce pig iron and high titania slag. The product, high titania slag can be converted to a white pigment through the chloride route, (Kahn, 1983). This project deals with the chlorination of such high titania slag.

2.3 Oxidation of High Titania Slag.

Because of the presence of trivalent titanium in high-titanium slag, the slag can undergo oxidation in the solid state, as shown by various studies.

Borowiec et. al. (1998) developed a method to upgrade several types of titania slag such as Sorelslag^{TM} with total Ti content (reported as TiO_2) in the range 78.30-84.80 weight % and Richards Bay slag of composition 86.20 weight % TiO_2. These slags are sized to a particle size range of 75-850 microns, and oxidised with an oxygen containing gas at a temperature of at least about 950^{O}C for at least 20 minutes. During this process, a substantial portion of the iron oxide and Ti_2O_3 are converted to the ferric and TiO_2 states respectively and the glassy silicate phase decomposes. The oxidised slag is then reduced at a temperature of at least 700^{O}C such that the ferric oxides are again converted to the ferrous state. The product is then leached with 20% excess of mineral acid at a temperature of at least 125^{O}C and one atmospheric pressure to yield the upgraded slag. The slag is then washed and calcined by heating to a

temperature in the range 600-800^{O}C. The product contains TiO_2 content in the range 93-96 wt %.

Vasyutinsky and Movsesov, (1965) studied the oxidation and grinding of titania slag containing 90.1%TiO_2 and 3.47%FeO. They concluded that to obtain the maximum reduction in strength of the slag, oxidation of the slag in the temperature region of 500-600^{O}C was required. Vasyutinsky, (1968) did an in-depth study of the oxidation of a similar high titania slag. The slag consisted mainly of a M_3O_5 phase, which could best be represented as x[(Fe, Mg, Mn)O. $2TiO_2$].y[(Ti, Al, Cr)$_2O_3$.TiO_2 solid solution. The experimental results on the oxidation of the slag indicated the following three main stages:

- At temperature of approximately 300-400^{O}C, only structural changes in the M_3O_5 phase was observed. X-ray diffraction analysis indicated a distortion of the M_3O_5 crystal lattice.
- At temperature $\leq$ 750^{O}C, the formation of anatase was observed.
- At higher temperature the formation of rutile was observed.

The anatase to rutile conversion temperature can range between 400-1000^{O}C, depending on the source of the anatase and type of impurities in it.

Bessinger et al. (2001) studied the decrepitation of solidified high titania slag. This was done by oxidising titania slag samples produced in a pilot plant furnace at temperature between 400 and 800^{O}C. During the slag cooling process, severe decrepitation of the slag may occur. This was detrimental to the slag because an excess of fine materials with average particle diameter of less than 106μm was produced. This lower valued products should be minimized in order to maximize the income that could be derived from titania slag. Decrepitation is defined as the disintegration or crumbling of a material into component parts or smaller fragments. Generally, decrepitation of slags occur due to phase and chemical changes in the slag and resultant volume changes associated with these phase changes, (Noguchi et al.,1980). Decrepitation of high titania slags was explained by oxidation of the M_3O_5 phase, resulting in the formation of anatase. As the density of anatase is less than the density of the M_3O_5 phase, this resulted in cracking of the slag (Vasyutinsky, 1968). Bessinger et al. (2001) confirmed that

decrepitation of titania slags was observed after heating at 400°C. They postulated that decrepitation occurs due to changes in the crystal lattice of the M_3O_5 phase in the slag due to oxidation .

2.4. Mineralogy and Phase Chemistry Of Titaniferous Feedstock

Ilmenite refers to the compound $FeTiO_3$, but naturally occurring ilmenite can also contain small amounts of MnO, MgO, Fe_2O_3 or Ti_2O_3 in its structure (van Dyk et al. 1999). As mentioned in section 1.1, four main mineralogical phases were identified to be present in the various high-titanium slags (Bessinger et al. 1997). The major phase is a solid solution phase referred to as M_3O_5 with end-members of the solid solution series such as $FeTi_2O_5$ (ferropseudobrookite), $MgTi_2O_5$ (armalcolite), and Ti_3O_5 (anosovite). The other three phases are rutile, metallic iron and a glassy phase (Bessinger et. al. 1997; Nell, 1999).

Table 2.4: Chemical Composition of Various Upgraded Titaniferous Feedstocks (van Dyk et al. 1999).

	TiO_2	FeO	MgO	Al_2O_3	CaO	V_2O_5	Cr_2O_3	MnO	SiO_2
Titania slag	86.4	10.5	1.00	1.00	0.13	0.42	0.11	1.71	1.58
Upgraded slag	94.9	2.47	0.67	0.46	0.06	0.35	0.06	0.03	1.69
Benelite synthetic rutile	93.8	4.83	0.02	0.51	0.05	0.08	0.02	0.05	1.34
Becher synthetic rutile	95.1	2.65	0.35	1.12	0.05	0.27	0.12	0.71	0.95

Van Dyk et al. (1999) reviewed the properties of some upgraded feedstocks, table 2.4. Of these, the feedstock with lowest TiO_2 content (86 %) and the highest impurity level was titania slag. The TiO_2 content of the other main feedstocks ranged between 93-95%. The main impurity in all the products was iron (as iron oxide). The levels of minor impurities in the product were all below

the levels specified for the chloride process, although the silica content in the titania slag and upgraded slag products may be too high for some chloride plants (van Dyk et al. 1999). As stated before, the slag consisted primarily of M_3O_5 (pseudobrookite) phase together with trace amounts of rutile. The Benelite synthetic rutile and upgraded slag products both have rutile as the main phase, with M_3O_5 present as trace phase. In the Becher synthetic rutile, Ti_3O_5 was the main phase along with rutile. M_3O_5, ilmenite and metallic iron were also present as minor and trace components (van Dyk et al. 1999). The trivalent titania (Ti_2O_3) occurs as a result of the highly reducing conditions applied in the Becher process to reduce all of the iron oxide to the metallic state. The M_3O_5 phase in the titania slag particles had a dense appearance and smooth texture.

2.4.1 Ti-O-Fe Phase diagram

A continuous solid solution series exists between $Fe_2^{3+}Ti_2O_5$ (ferripseudobrookite), $Fe^{2+}Ti_2O_5$ (ferropseudobrookite) and $Ti^{4+}Ti_2^{3+}O_5$ or Ti_3O_5 (anosovite) at temperatures above 1320^{O}C. The end members of these solid solutions are unstable at low temperatures. As reported by Eriksson et. al. (1996), ferripseudobrookite decomposes to rutile and hematite below 585-/+5^{O}C, while ferropseudobrookite decomposes below 1140+/-10^{O}C to rutile and ilmenite.

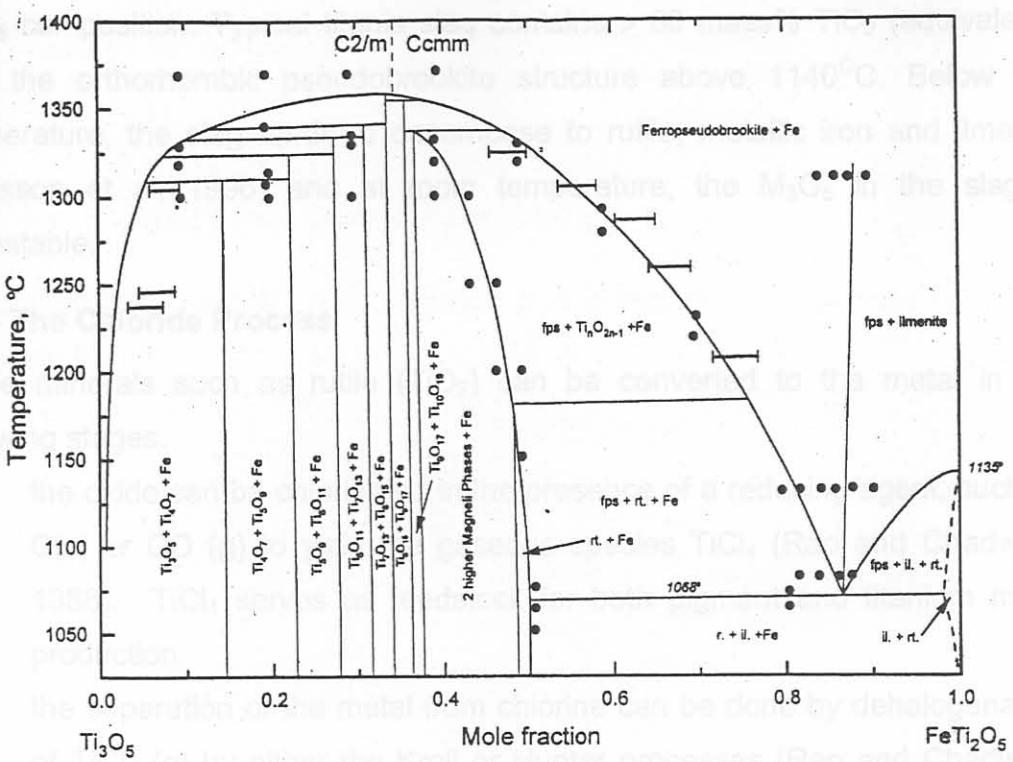

Figure 2.4.1: Binary Section $FeTi_2O_5$-Ti_3O_5 through The Fe-Ti-O Phase Diagram (Eriksson et al. 1996)

Eriksson et al. (1996) investigated the stability of pseudobrookite type solid solutions in the binary section $FeTi_2O_5$-Ti_3O_5 of the Fe-Ti-O phase diagram. They found that, towards higher titanium concentrations, the solid solution based on Ti_3O_5 decomposes below the solvus line to give a series of Magneli phases as seen in figure 2.4.1. These Magneli phases have the general formula Ti_nO_{2n-1} where $4 \leq n \leq 10$. (Eriksson et al. 1996).

These series of solid solution were also studied by Grey et al. (1973) for variations in temperature and oxygen partial pressure. They found that the solid solution was complete at temperatures above 1350°C. For the series $Fe_xTi_{3-x}O_5$ (with $0 \leq x \leq 1$) it was found that with $x > 0.35$ the compounds have an orthohombic pseudobrookite structure. With $x < 0.35$ the compounds have a monoclinic distortion of this structure, with the distortion increasing towards the

Ti_3O_5 composition. Typical titania slag contains > 80 mass% TiO_2 (equivalent), with the orthorhombic pseudobrookite structure above 1140^{O}C. Below this temperature, the slag tends to decompose to rutile, metallic iron and ilmenite (Eriksson et al. 1996) and at room temperature, the M_3O_5 in the slag is metastable.

2.5 The Chloride Process

Oxide minerals such as rutile (TiO_2) can be converted to the metal in the following stages.

i. the oxide can be chlorinated in the presence of a reducing agent, such as C(s) or CO (g) to yield the gaseous species $TiCl_4$ (Rao and Chadwick, 1988). $TiCl_4$ serves as feedstock for both pigment and titanium metal production.

ii. the separation of the metal from chlorine can be done by dehalogenation of $TiCl_4$ (g) by either the Kroll or Hunter processes (Rao and Chadwick, 1988), reactions 2.5a and b.

$$TiCl_{4\,(g)} + 2Mg_{\,(l,\,g)} \rightarrow Ti_{(s)} + 2MgCl_{2\,(l)} \text{ (Kroll process)} \text{----------2.5a.}$$

$$TiCl_{4(g)} + 4Na_{(l,g)} \rightarrow Ti_{(s)} + 4NaCl_{(l)} \text{ (Hunter Process)----------2.5b.}$$

iii. The titanium sponge can then be purified by high temperature distillation under vacuum or by an inert-gas sweep. The residual salts can also be removed by the leaching of the sponge (Rao and Chadwick, 1988).

2.5.1 Fluidized Bed Reactor

A fluidised bed reactor was used in this project for the chlorination of oxidized titania slag, hence the underlying principle of the reactor is discussed below.

In the reactor, a bed of finely divided solids is lifted and agitated by a rising stream of gas or liquid. At low gas velocities, the lifting effect of the bed is slight and the system behaves like a boiling liquid. With increasing velocity, the

proportion of particles entrained in the gas stream also increases until at some point the gas carries away all particles fed into the bed (Szekely and Themelis, 1971).

2.5.1 i Fluid Flow Through Packed Beds

The simplest representation of a packed bed is that of a vertical tube filled with particles of a uniform size; see Fig 2.5.1 below.

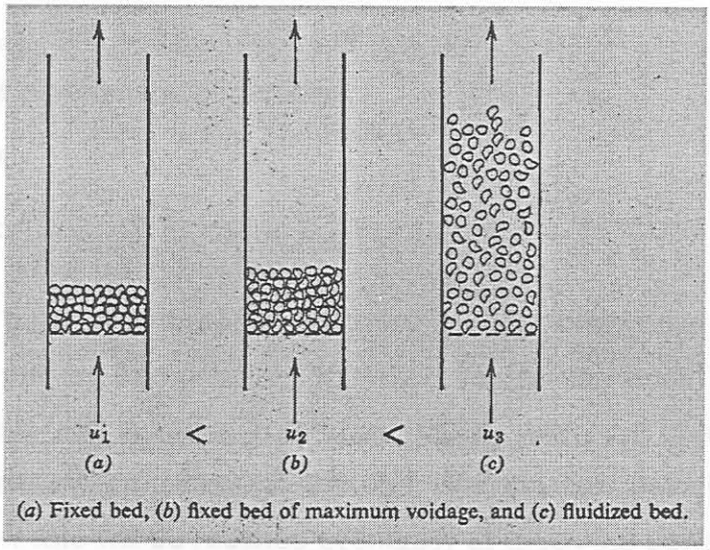

(a) Fixed bed, (b) fixed bed of maximum voidage, and (c) fluidized bed.

Fig 2.5.1: a.) Fixed bed, b.) Fixed bed of maximum voidage, c.) Fluidized bed (Szekely and Themelis, 1971).

The constitution of the bed is characterized by the following parameters: void fraction or voidage (ε), particle size and particle shape factor,

Where Voidage (ε) = (total volume of bed – volume of solid particles)/total volume of bed. ----------2.5.1a

The size of a nonspherical particle may be expressed in terms of the volume equivalent diameter defined as,

d_p = diameter of a sphere of equal volume to particle (cm). ---- 2.5.1b

For solids of irregular shape but exhibiting roughly spherical symmetry, the mesh size determined by sieving is a good approximation of the equivalent volume

diameter. However, in many cases, it is necessary to define the deviation of the shape of a particle from a sphere quantitatively, by mass of a correction factor, which is called the shape factor (Φ_s) given as

Φ_s = Surface area of sphere of equal volume to particle/Surface area of particle. ----------2.5.1c

For spherical particles;

Φ_s =1

for other shape of particle;

Φ_s < 1.

2.5.1 ii Fluid Flow in Fluidized Beds

The nature of fluidization may be illustrated by considering the upward flow of gas through a packed bed of solid, Figure 2.5.1a (Szekely and Themelis, 1971). At low flow rates, any increase in the gas velocity will result in a corresponding increase in pressure drop through the bed. As the fluid velocity is increased gradually, a flow rate will be reached eventually at which the upward force due to the pressure drop across the bed is equal to the weight of the particles in the bed. At this stage, the particles become rearranged so as to offer less resistance to fluid flow and the bed expands, Figure 2.5.1 b. The expansion continues with further increase in gas velocity, until the bed assumes the loosest possible packing. At even higher gas velocity, the particles become freely suspended in the gas stream. Under these conditions, the bed is said to be in a fluidized state, Fig 2.5.1 c. From a macroscopic point of view, a gas-solid fluidized bed may be regarded as a well stirred, boiling liquid. Because of the high degree of mixing of the solids, it is relatively easy to maintain uniform temperatures within the bed. This ready control of temperature, plus the facility of handling the solid feed and product as pseudofluids, has resulted in the wide use of fluidized beds as reactors for highly exothermic and endothermic reactions (Szekely and Themelis, 1971).

2.5.1 iii Minimum and Maximum Fluidization Velocity

The minimum fluidization velocity denoted U_{mf} is the velocity at which the pressure drop across the bed is equal to the weight of the solid particles. It is derived from the following:

$$A_B g\Delta P = A_B L_{MF}(1-\varepsilon)g(\rho_s - \rho_g) \text{ ----------2.5.1d}$$

Where
- ΔP = Pressure drop across the bed
- A_B = Cross-sectional area of the bed
- L_{mf} = Depth of bed at point of minimum fluidization
- ε_{mf} = Bed voidage at point of minimum fluidization
- ρ_g = Density of gas
- ρ_s = Density of solid
- g = acceleration due to gravity

Elutriation or maximum fluidization velocity (denoted U_t) is defined as the upper limit of gas velocities in a fluidized bed. In other words, it is the velocity at which a particle is entrained and carried away from the reactor in the gas stream and may be assumed to be the terminal falling velocity of the particles. The following expressions can be use to calculate the elutriation velocity depending on the Reynold number (N_{Rep}).

$$U_T = [d_p^2 g(\rho_s - \rho_g)]/18\mu \quad for\ N_{Re\,p} < 0.4 \text{ ----------2.5.1e}$$

$$U_T = 0.0178[g^2(\rho_s - \rho_g)^2 / \rho_s]^{1/3} d_p \quad 0.4 < N_{Rep} < 500 \text{ ----------2.5.1f}$$

$$U_T = [3.1 d_p g(\rho_s - \rho_g)/\rho_g]^{1/2} \text{ for } 500 < N_{Rep} < 2*10^5 \text{ ----------2.5.1g}$$

If we wish to minimise the amount of elutriation by the gas stream, the operating velocity U_O must lie between the minimum and maximum fluidisation velocities.

Different authors used various flow rates in their laboratory fluidized-bed chlorinators. Morris and Jensen, (1976) when chlorinating rutile, used a flow rate 10 times the minimum fluidizing velocity resulting in an equivalent linear gas velocity of 24cm/s, that is 6l/min at 25^{O}C through a 4.75cm inside diameter reactor tube. Sohn and Zhou, (1998) when chlorinating slag used a flow rate 10 times the minimum fluidizing velocity that resulted in a volumetric flowrate of 900cm^3/min at 25^{O}C in a 2.5cm inside diameter reactor tube. In the above cases, the average particle size was approximately the same, being 163μm and 177μm respectively.

2.5.2 Nature and Feedstock Requirements of the Chloride Process

The chloride process is a continuous one that operates in a fluidised-bed reactor. The raw material must have:

- Sufficient grain size and bulk density to minimize blow-over in the chlorination fluidized-bed reactor. In other words, most of the unreacted rutile and coke should not be carried over with the $TiCl_4$ (Minkler and Baroch, 1981). In this respect, natural rutile has an advantage over synthetic rutile, since the latter has a porous grain structure and lower bulk density (Stanaway, 1994).
- very low alkali earth metal content, especially MgO and CaO. Alkali earths form liquid chlorides at the chlorination temperatures. The liquid chlorides can defluidise and clog the reactor bed. In other words the liquid chlorides would block the pores of the fluidised bed thereby preventing free flow of the gas mixture, which may result in a large pressure drop in the lower part of the reactor. In addition, together with chromium, alkalis also act as fluxes promoting bed fusion (Stanaway, 1994). Also CaO reduces the chlorination of TiO_2 and SiO_2 by forming $CaO.TiO_2$ (Minkler and Baroch, 1981).

These effects are due to the fact that the chlorides of Mg and Ca have high boiling points (Minkler and Baroch, 1981) see table 2.5.2.

Table 2.5.2: Melting and Boiling Points of Chlorides of Calcium, Magnesium, Iron and Titanium, Sigma-Aldrich.

	$CaCl_2$	$MgCl_2$	$FeCl_3$	$TiCl_4$
Melting points (^{O}C)	782	714	306	-24.1
Boiling points (^{O}C)	1600	1412	316	136.4

- Low iron content to minimize the iron trichloride disposal problem, optimize plant capacity and minimize reagent consumption. $FeCl_3$ is a low boiling point impurity, which must be concentrated and removed in the purification stage by distilling out $TiCl_4$ or by centrifugation. High iron content in the ore will make it more difficult to concentrate and produce pure $TiCl_4$ gas (Stanaway, 1994 ; van Dyk et. al. 1999).
- Minimal chromium and vanadium, which impart potential toxicity to iron chloride waste (Stanaway, 1994 ; van Dyk et. al. 1999).
- Low silica, which could coat titanium minerals grains and so prevent their reaction with chlorine (Stanaway, 1994 ; van Dyk et. al. 1999). .
- Low tin and arsenic, which are difficult to separate in purification steps and which accumulate in the purified titanium tetrachloride (Stanaway, 1994 ; van Dyk et. al. 1999).
- Minimal uranium and thorium due to their undesirable radioactivity (Stanaway, 1994 ; van Dyk et. al. 1999).

2.5.3 Chlorination Kinetics of Titaniferous Feedstocks.

Rowe and Opie, (1955) reviewed the production and purification of titanium tetrachloride vapour. They used natural rutile feed (95% TiO_2) and chlorine in the presence of carbon at 700^{O}C in static-bed and fluidised-bed reactors. Briquettes of carbonised rutile-coke mixtures were fed at intervals to the stationary chlorination furnace, which was maintained at a temperature of 800^{O}C. Electrical energy supplied through carbon electrodes was used to supplement the heat produced during the reaction. Chlorine gas was introduced at a level slightly below the electrodes and as the chlorine rose through the furnace it reacted with the TiO_2-C briquettes. The gaseous product was led through the

dust catchers to a $TiCl_4$ condenser. The main disadvantages of the static-bed reactors are that they are discontinuous and they have to be periodically shut down to remove the residue or ashes that remained from the chlorination.

Modern plants make use of fluidised-bed reactors with closely sized solid feed materials (rutile, slag, ilmenite, and coke) to produce gaseous $TiCl_4$ (Rao and Chadwick, 1988; Stanaway, 1994; van Dyk et. al. 1999). In this type of reactor, the bed is usually supported on a perforated brick or ceramic plate. The titaniferous feedstock and coke are charged through a port above the bed (Rowe and Opie, 1955). The latter is kept in a fluidized state by the incoming reactive gas stream (Cl_2), which is admitted at high pressure. A small amount of N_2 is mixed with the input gas stream to regulate the temperature of the bed. Excellent heat transfer and high production rates make fluidised-bed reactors very attractive. The principal reactions in the chlorination of $TiO_{2(s)}$ are:

$$TiO_{2(s)} + 2C_{(s)} + 2Cl_{2(g)} \rightarrow TiCl_{4(g)} + 2CO_{(g)} \quad (T > 700^{O}C) \text{----------} 2.5.3a.$$

$$C_{(s)} + CO_{2(g)} \rightarrow 2CO_{(g)} \quad \text{(Boudouard reaction)} \text{----------} 2.5.3b.$$

$$TiO_{2(s)} + 2CO_{(g)} + 2Cl_{2(g)} \rightarrow TiCl_{4(g)} + 2CO_{2(g)} \text{----------} 2.5.3c.$$

For chlorination with a solid carbon reductant (equation 2.5.3a) above 700 ^{O}C CO is the dominant carbonaceous off-gas species.

Dunn, (1960) studied the chlorination rates of several titanium-containing materials in CO-Cl_2 gas mixture. He found that the chlorination rate of rutile depended linearly on the partial pressures of CO and chlorine in both fixed and fluidised–bed reactors. The rate expression relating the fraction of rutile chlorinated and the partial pressures of the two gases used is given as:

$$X = 55P_{CO}P_{Cl2}EXP[(-1.05 X10^{4})/T]t \text{----------} 2.5.3d$$

Where X = Fraction of rutile chlorinated
T = Temperature in Kelvin
P = partial pressures in atm
t = Time in minutes.

Bergholm, (1961) chlorinated Australian rutile in the presence of CO and carbon. For the CO-Cl_2 system, he found that the rate of reaction was proportional to the CO concentration but independent of Cl_2 concentration. The activation energies for these reactions are given in the table 2.5.3a below.

Table 2.5.3a: List of activation energies for the chlorination of titanium feedstock in different gas mixtures

Authors	Sample type	Reaction system	Activation energy (kJ/mol)	Temperature ranges (K)
Bergholm (1961)	Rutile	CO-Cl_2	104	
Dunn (1960)	Rutile & beneficiated ilmenite ("synthetic rutile")	CO-Cl_2	87.5	
Morris and Jensen (1976)	Rutile	CO-Cl_2	158	1143-1311
Morris and Jensen (1976)	Rutile	C - Cl_2	45.2	1143-1311
Sohn and Zhou (1999)	Rutile	CO-Cl_2	175	
Sohn and Zhou (1999)	beneficiated ilmenite ("synthetic rutile")	CO-Cl_2	156	
Jena et al (1998)	Pure TiO_2	C - Cl_2	130	773-873
Jena et al (1998)	Pure TiO_2	C - Cl_2	12	973-1273
Pistorius and le Roux (2002)	Titania slag	CO-Cl_2	28.8	1223
Sohn and Zhou (1998)	Titania slag	C - Cl_2	29	

Morris and Jensen, (1976) measured the porosity and density of Australian rutile particles at various degrees of chlorination. The results showed that Australian rutile was a non-porous solid, which undergoes no internal chlorination. Therefore, the reaction occurred exclusively at the surface of the particle at a rate proportional to the receding surface area. They developed an empirical equation based on the experimental results in both the $CO\text{-}Cl_2$ and $C\text{-}Cl_2$ systems respectively. The rate expressions they obtained are;

$(1-(1-X_B)^{1/3})/\theta = 6065(P_{CO}P_{Cl2})^{0.665}EXP(-37{,}800/RT)$----------2.5.3e

$$\left(1-(1-X_B)^{1/3}\right)/\theta = 0.294(P_{CO}^{0.692}d_C^{-0.55})(Coke/Ore)^{0.376}Exp\left(-10{,}820/RT\right)$$ --2.5.3f

Where k = rate constant

θ = Run time in minutes

d_c = Diameter of carbon particle (in cm)

P = Partial pressure (in atm(1.013×10^5 Pa))

X_B = fractional conversion

T = Reaction temperature (in K)

R = Universal gas constant (1.99 cal mol^{-1} K^{-1}).

The fractional order kinetics implied by the partial pressure exponents suggested that the TiO_2 surface was covered with relatively stable primary reaction products such as $TiCl_2$ and $TiOCl_2$, which limit the access of CO and Cl_2 to the surface, thereby reducing the apparent order of the reaction (Morris and Jensen, 1976). This could be attributed to the non-porous nature of rutile after the first few minutes of chlorination. Zhou et al. (1996) reported that further chlorination after the first 15 minutes leaves the rutile surface with some small grains, which are not properly oriented to react. It was also noted that natural rutile particles were more crystalline than synthetic rutile and thus undergo fewer microstructural changes during the chlorination reaction. Morris and Jensen, (1976) showed that, in the chlorination of Australian rutile, the activation energy for the $C\text{-}Cl_2$ system was very low compared to that of the $CO\text{-}Cl_2$ system with equal partial

pressure of chlorine. This result showed that, for rutile, coke was a more effective chlorination promoter than CO. At 1273K the rate with coke was nineteen times faster than that with CO as the reducing agent when chlorinating rutile. In the C-Cl_2 system, it was observed that the rate increases with increased coke/ore ratio (Morris and Jensen, 1976), equation 2.5.3f. However, for a fixed fluidised-bed volume, the amount of ore decreases correspondingly, so that there should exist an optimium coke/ore ratio for maximum efficiency of chlorine removal. The result of this study has been applied to minimize the chlorine losses in and preparing a comprehensive model of commercial fliudized-bed chlorinators (Morris and Jensen, 1976).

Recently, Jena et al. (1998) did a study on the kinetics of the carbothermic chlorination of fine TiO_2 powder (-32 to 25μm) by gaseous chlorine in a mixture with graphite powder (20-50 weight %) of the same particle size. The experiment was performed over two different temperature ranges, 773-873K and 973-1273K. They found that the fine powder of pure titanium dioxide mixed in a weight ratio of 3:2 with equally fine powdered pure graphite could be chlorinated appreciably (88%) in 75 minutes, even at the low temperature of 873K. They also found that unlike with CO, the amount of TiO_2 chlorinated increased with increase in the proportion of graphite up to 40 weight % after which the rate dropped. Chlorination, whether in the low (773-873K) or high (973-1273K) temperature ranges follows the topochemical reaction model as shown in equation 2.5.3g.

$$1-(1-\alpha)^{1/3} = Kt \text{----------} \quad 2.5.3g$$

Where α = fraction of TiO_2 reacted.
t = times in minutes
K = rate constant in min^{-1}

This indicated that the graphite must have taken part in the reaction directly (as the initial chlorination rate of TiO_2 was directly proportional to the initial amount of the graphite) and the decrease in the $\%TiO_2$ chlorinated at more than 40 weight

% graphite might be attributed to partial segregation between the particles because of the difference in their densities.

In all cases, the topochemical reaction model given in equation 2.5.3g provided a good fit to the amount of TiO_2 chlorinated (Jena et al., 1998). In the lower temperature range, the rate of chlorination was found to be proportional to P_{Cl2}, with activation energy of 130kJ/mol. The formation of the solid intermediate ($TiCl_2$) (reaction 2.5.3h), was suggested to be the rate-determining step in the lower temperature range (Jena et al. 1998). In the higher temperature range, the rate was proportional to the square root of P_{Cl2}, and reaction 2.5.3i was suggested to be the rate-determining step with activation energy as low as 12kJ/mol, since the production of $TiCl_2$ was considered to be fast. Experimental evidence for the formation of $TiCl_2$ had been provided by Zhou et al. (1996) who showed (using X-ray diffraction) that the final product on the surface layer was a solid solution of TiO and a small amount of Ti_3O_5.
Jena et al. (1998) suggested that the mechanism of the reaction was as follows:

$$TiO_{2(s)} + C_{(s)} + Cl_{2\,(g)} \rightarrow TiCl_{2(S)} + CO_{2\,(g)} \text{ ----------2.5.3h}$$

$$TiCl_{2(S)} + 1/2Cl_{2(g)} \rightarrow TiCl_{3(s)} \text{ ----------2.5.3i}$$

$$TiCl_{3(s)} + 1/2Cl_{2(g)} \rightarrow TiCl_{4\,(g)} \text{ ----------2.5.3j}$$

Finally, formation of the most stable gaseous phase, $TiCl_4$, according to reaction 2.5.3j, was considered to be fast under the reaction condition (Jena et al. 1998).
Rao and Chadwick (1988) studied the rate of chlorination of synthetic rutile in CO-Cl_2-He gas mixtures by thermogravimetry in the temperature range of 500-1000 ^{o}C. The synthetic rutile was prepared by oxidising a thin titanium metal foil. They found that the exponents for the partial pressures of CO and Cl_2 varied with the reaction temperature. They also found that phosgene ($COCl_2$) was formed when chlorine and carbon monoxide were mixed with each other under visible

light; this caused an anomaly in the experimental results below 800^{O}C. Above this temperature, phosgene decomposes and does not have any effect on the chlorination reaction.

Sohn and Zhou, (1999) showed that beneficiated ilmenite ("synthetic rutile") was a porous material. It is quite different from natural rutile, hence has a different chlorination rate. The sample used in their experiments was obtained by the Becher process (containing 92%TiO_2, 4%FeO, and 1% each of alumina, silica and magnesium oxide). During chlorination it was observed that the amount of titanium chlorinated at a given time increases with decreasing particle size, although the effect was not as large as that of natural rutile. The small dependence on superficial particle size was due to the presence of porosity. The shrinking core model was not applicable in this case, because the sample was porous and thus pore diffusion occurred simultaneously with chemical reaction inside the particle, which does not allow a topochemical reaction. The most appropriate rate expression was a pore-blocking rate law that gave the most satisfactory correlation of the results and is given as:

$K_{app}t = \lambda[\exp(x/\lambda)-1]$ ----------2.5.3k

Where x = fraction of TiO_2 converted

K_{app} = apparent rate constant

λ = constant independent of conversion

t = time in minutes

λ was related to the blockage, which inhibits access of reactant gases.

The origin of this relationship could be attributed to the numerous pores formed during beneficiation of the synthetic rutile (Sohn and Zhou, 1999). They also carried out experiments with various mixtures of carbon monoxide and chlorine gases to investigate the effect of partial pressures on the reaction rate at 900^{O}C. The particle size of the beneficiated ilmenite was 150-212μm. They found that the apparent rate constant, K_{app} , was a function of the partial pressure of the reactant gases and does not depend on particle size. They observed that the

rate of chlorination increases as the partial pressure of both CO and Cl_2 increases with chlorine giving a greater influence on the rate than CO. The rate expression in term of the Pco and P_{Cl2} is given as;

$$Kapp = KP_{CO}^{m} P_{Cl2}^{n} \text{ ---------- } 2.5.3l$$

Substituting equation 2.5.3l into equation 2.5.3k gives the overall rate expression for the reaction in terms of Pco and P_{Cl2}:

$$\lambda[\exp(x/\lambda)-1]-b = KP_{CO}^{0.82} P_{Cl2} t \text{ ---------- } 2.5.3m$$

Where b = $3.32d_p^{-0.8}$

d_p = particle size.

The rate of the chlorination reaction was also found to increase with temperature, and an apparent activation energy of 156kJ/mol was observed (Sohn and Zhou, 1999).

Zhou et al. (1996) investigated the effect of reaction time on the chlorination of ground titania slag particles with petroleum coke in a fluidized bed. The surfaces of the original slag particles contained no pores. When the samples were chlorinated at 1393K the % titanium and % iron chlorinated with time is given in the table 2.5.3b.

Table 2.5.3b: Effect of reaction time on the degree of chlorination of titania slag at 1393K[a].

Reaction time (min)	% titanium chlorinated	% iron chlorinated
15	11	70
30	28	80
90	95	99

a = Gas mixtures containing nitrogen, carbon monoxide and chlorine were used and the average particle size of the slag was 125μm.

At the end of the reaction time, SEM/EDX analysis showed that the surface was covered with small crystallites about 3μm in diameter. These crystallites were

composed mainly of rutile with small amounts of SiO_2, MgO, sometimes Al_2O_3, but no iron oxides. The chlorination reaction started with the easily chlorinated elements such as iron exposed on the surface leaving the particle surface with pores, crystallites of TiO_2 and other chlorination-resistant oxides. The outer shell was depleted of TiO_2 and gradually enriched with impurities that hinder the reaction by inhibiting the gas diffusion. This was confirmed by electron probe microanalysis (EPMA) of the particle cross-section which showed the elemental distribution where the unchlorinated impurities containing silica collected largely at the outer shell of the particle with the unreacted core consisting of TiO_2.

They also showed solid–state sintering and grain growth during the process at high temperature (1323K). At low temperature (1223K) the individual grains were very distinct while at intermediate temperature (1273K) a mixed microstructure was observed. It was apparent that, at lower temperature, the crystallites were larger than at higher temperatures. This may be partially due to the fact that lower temperature benefits the chlorination of iron relative to that of TiO_2 and partially due to the fact that, at lower temperatures, grain growth and sintering were slow. The significance of this is that a substantial amount of iron oxide contained in titania slag contributes significantly to the difference in the way the morphology of the solid changes during the chlorination reaction. When rutile is chlorinated, the generated surface morphology is largely limited to a narrow layer near the external surface. In the case of titania slag, the rapid chlorination of easily chlorinated iron oxide creates porosity that extends deeply into the interior of the particles. The remaining titanium oxide phase has a much greater surface area on which the chlorination reaction can occur. Thus, the rate of chlorination of titanium slag per unit area of the apparent external surface was expected to be considerably higher than that of rutile. The fact that a porous structure was established quickly by the chlorination of the easily chlorinated components was confirmed by the result of the B.E.T. specific surface area measurement. It showed that the surface area remained largely unchanged during the reaction after the rapid initial increase.

Sohn and Zhou, (1998) investigated the effect of temperature, chlorine partial pressure and the original slag size on chlorination rate (with coke as reductant). They found that, as the chlorine partial pressure increases, the rate of chlorination increases significantly with a reaction order of 1.5. The initial particle size of the slag was found to have a very limited effect on the rate of reaction. An increase in temperature was found to favour the rate of chlorination even though the effect was small with a very low activation energy of 29kJ/mol, table 2.5.3. Initially, the rate of reaction increased significantly, but as the reaction proceeded, this rate increase becomes less significant. This can be explained from the fact that the specific surface area of the slag increases tremendously after the first few seconds of the reaction, causing the rate of the reaction to increase. This can be attributed to the fact that, the slag becomes highly porous as the FeO in the slag is chlorinated (Zhou et al. 1996). The small induction time (t_o) at the beginning of the reaction, which mainly represents the time for the chlorination of the iron oxide and manganese oxide to create the porous titanium dioxide structure, increased with decreasing temperature (Sohn and Zhou, 1998). The relationship between the induction time and temperature is given as:

$t_o = 0.04\exp(6900/T)$ ----------2.5.3n

where t_o = induction time

t = time in minutes

T = Temperature in Kelvin

The chlorination rate of titania slag with petroleum coke in a fluidised-bed reactor can be summarized as:

$1-(1-X)^{1/3} = K_{app}(t-t_o)$, $t>t_o$ ----------2.5.3o

Le Roux, (2001) constructed a laboratory scale chlorinator which was used to compare the chlorination behaviour of block route slag to the literature data on rutile. The schematic diagram of the experimental set-up used is given in Fig 2.5.3a below.

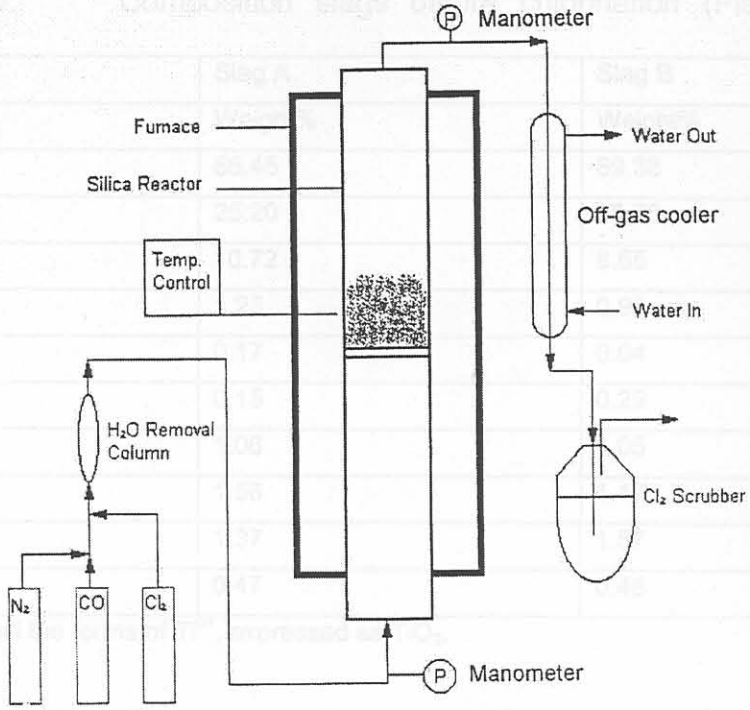

Fig 2.5.3a: Schematic Diagram of Laboratory Chlorinator (le Roux, 2001)

With the laboratory chlorinator, Pistorius and le Roux, (2002) determined the thermal, chemical and structural changes during initial chlorination of two block route slags whose compositions are given in table 2.5.3b.

Table 2.5.3b: Composition slags before chlorination (Pistorius and le Roux, 2002)

Compound	Slag A	Slag B
	Weight%	Weight%
TiO_2*	86.45	89.38
Tl_2O_3	25.20	33.70
FeO	10.72	8.65
Al_2O_3	1.23	0.93
Cr_2O_3	0.17	0.04
CaO	0.15	0.29
MgO	1.06	1.05
MnO	1.56	1.17
SiO_2	1.37	1.57
V_2O_5	0.47	0.48

TiO_2* denotes all the forms of Ti^{n+}, expressed as TiO_2.

The differences between these two slags are mainly in the Ti_2O_3 and FeO contents. In determining the effect of Ti^{3+} on chlorination of the slag they showed that Ti^{3+} (Ti_2O_3) in the slag acts as a reductant, and hence contributes to the chlorination of MnO and FeO present.

It was also shown that, in addition to its role as reductant, Ti_2O_3 was also chlorinated to $TiCl_4$, equation 2.5.3p

$$2CO + Ti_2O_3 + 4Cl_2 \rightarrow 2TiCl_4 + 3CO_2 \qquad \Delta H = -876.8 \text{ kJ/mol----------2.5.3p}$$

All these reactions were highly exothermic and the heat evolved could cause the fluidized bed to sinter and create hotspots in the bed. It was noticed that the bed temperature rose dramatically in the beginning of the experiments. This is illustrated in Fig 2.5.3b for the two slags.

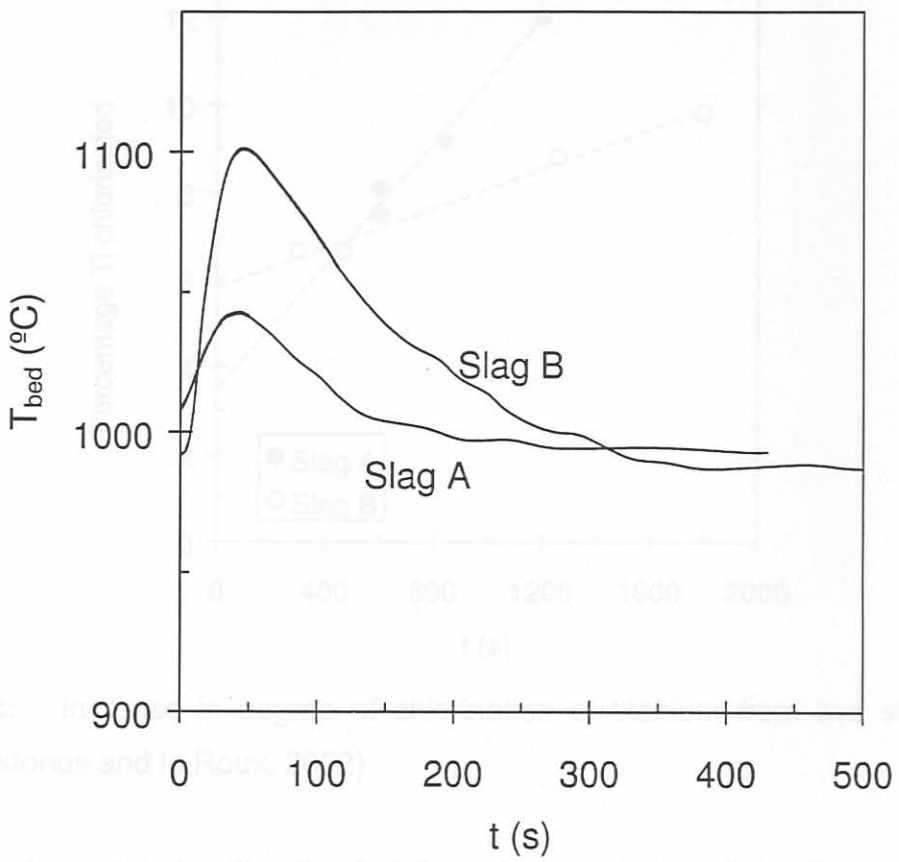

Figure 2.5.3b: Bed Temperature during Initial Chlorination of Slag A and B (Pistorius and le Roux, 2002).

It was shown that this rise was due to the presence of Ti_2O_3; the peak temperature depended on the amount of Ti_2O_3 present in the slag. Hence, a limited amount of Ti_2O_3 should be allowed in the slag.

They found that, the % of titanium chlorinated increases slowly with time (Fig 2.5.3c).

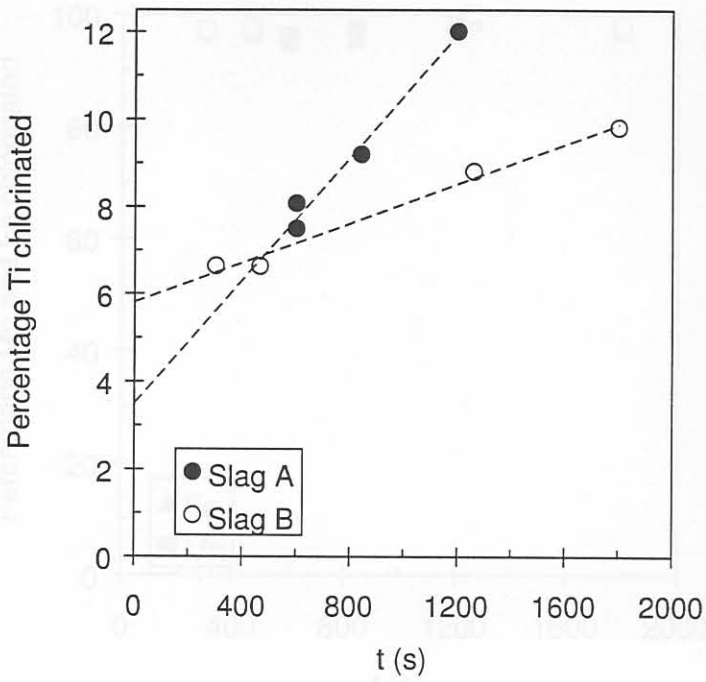

Fig 2.5.3c: Increase in degree of chlorination of titanium from two slags at 950°C (Pistorius and le Roux, 2002)

They also showed that, within the first five minutes, almost all the Fe and Mn in the slag were chlorinated (Fig. 2.5.3d). This was evident visually from the off-white appearance of the chlorinated slag, unlike the initial near-black particles. XRD analysis of the partially chlorinated samples showed the main crystalline phase to be rutile.

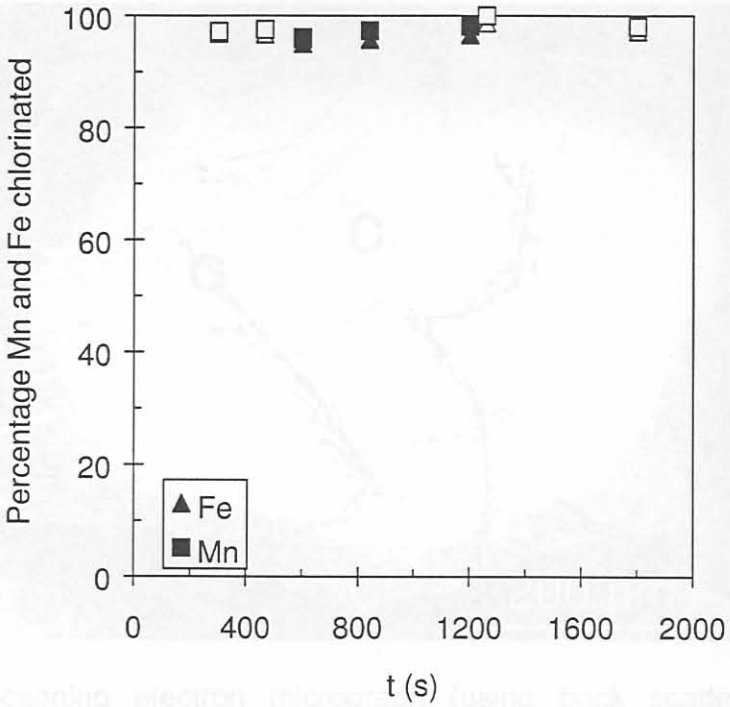

Fig 2.5.3d: Increase in the degree of chlorination of iron and manganese from slag A and B at 950 ^{O}C. Closed symbols are for slag A and open symbols for slag B, (Pistorius and le Roux, 2002).

The structural and compositional changes during the early chlorination of titania slag was also investigated. Results showed that a clear reaction front at the periphery of the particles was found during the first 30 seconds of chlorination. The front moves toward the particle centres at a rate of some 100μm/min. The chemical analyses showed that, ahead of the reaction front (towards the particle centre), the slag was unreacted whereas behind the reaction front it is essentially rutile (TiO_2), Fig 2.5.3e. The rutile matrix was highly porous due to the fast chlorination of oxides like FeO and MnO within the first few minutes of the process (Pistorius and le Roux, 2002). This agrees with the previous results, which showed that the chlorination of titania slag follows the topochemical reaction model (Zhou et al. 1996)

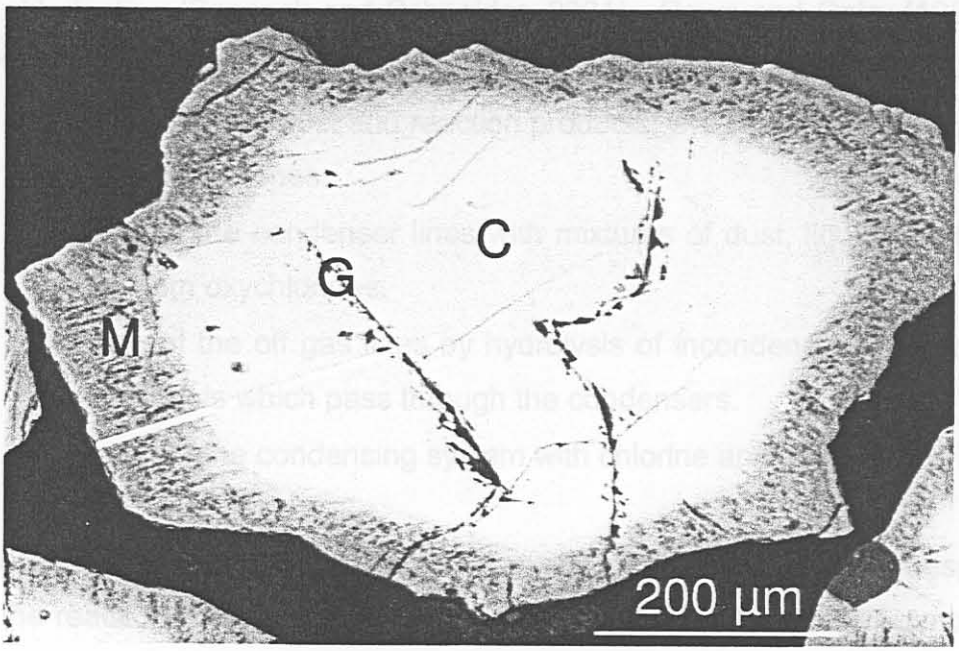

Fig 2.5.3e: Scanning electron micrograph (using back scattered electron imaging) of block route slag chlorinated for 30 seconds (Pistorius and le Roux, 2002).

2.6. Limitations of Fluidized-bed Technology and Possible Alternatives

Although fluidised-bed technology is used to produce titanium tetrachloride, there are strict feedstock requirements that limit the use of fluid-bed processing (Stanaway, 1994 ; van Dyk et al., 1999). Titanium ore feedstocks must fall within a narrow particle size range. Too-small particles will be elutriated from the fluidised-bed before sufficient residence time for the reaction, and too-large particles are difficult to fluidize. As stated before, the feedstock should contain very low amounts of alkaline earth metals, especially calcium oxide and to a lesser extent magnesium oxide. These chlorinate to form low vapour pressure or high boiling point liquid metal chlorides that tend to build up in the fluidised-bed. This could lead to defluidization, localised overheating and fusion of the bed. Also, the feedstock should contain low levels of chlorination inert components such as silica, which tend to accumulate in the bed and insulate the slag particles

from chlorination (Bonsack and Schneider, 2001). Rowe and Opie, (1955) also reported that the limitation of fluidised bed technology could be attributed to:

- Carry-over of fine dust and reaction products, which could only be partially removed by cyclones.
- Plugging of the condenser lines with mixtures of dust, liquid tetrachloride and titanium oxychlorides.
- Clogging of the off gas lines by hydrolysis of incondensable tetrachloride fogs and mists which pass through the condensers.
- Corrosion of the condensing system with chlorine and hydrochloric acid.

Rowe and Opie, (1955) showed that leakage of air into the system especially near the reaction zone could caused the oxidation of $FeCl_3$ and $TiCl_4$ to produce very fine Fe_2O_3 and TiO_2 particles, while moisture leakage will produce solid titanium oxychloride. Mechanical dust carry-over could be eliminated by careful charge preparation, close regulation of gas flows and adequate cyclone design (Rowe and Opie, 1955). They also mentioned that thorough drying of the charge and maintaining the system under a slight positive pressure could minimize these effects. Cooling of the exhausted gas mixture by refrigeration greatly reduced fog formation and minimized plugging in the system (Rowe and Opie, 1955).

Cole and Rowe, (1962) reported a flash chlorination technique capable of handling the unreacted fines. By charging the finely divided charge material of size between one and 50 microns into the bottom of the reactor bed chlorination occurs before the dust could pass through the bed.

Bonsack and Schneider, (2001) also showed that entrained-flow technology was a feasible alternative to the fluidised-bed process for producing titanium tetrachloride from feedstocks that are high in alkaline earth metals and chlorination inert components and that have a small particle size.

2.8. Conclusions

Despite the disadvantages of fluidised-bed technology, the method was used in this study for the chlorination of oxidised titania slag because of the following reasons. Firstly, the excellent heat transfer and high production rates make the reactor very attractive (Rao and Chadwick, 1988). Secondly, all chloride-route pigment producers use fluidised-bed chlorination reactors operating at 1000^{O}C or higher (Reeves and Reeves, 1997). Finally, the entrained-flow technology may be a feasible alternative but the method is new and has not yet been used by pigment producers (Bonsack and Scheider, 2001). However, one could recommend that more study be done on the entrained-flow method and how it can replace the fluidised-bed technique in the future.